J Nanostruct 16(4): 5859-5877, Autumn 2026

RESEARCH PAPER

Selenium Nanoparticles Restore GPX4 and Attenuate Ferroptosis-Associated Lipid Peroxidation While Modulating FGF21/Irisin Signalling in Insulin-Resistant Rats

Mohammed Ahmed Mustafa [1]*, Layla Abd Alsattar Sadiq Laylani [2], Adeeb M. F. Al-Samarrai [3], Sanan Thaer Abdalwahab [4], Esraa Ahmed Abdul Qader [5], Weam Wael Salman [6]

[1] *Department of Biology, College of Education for Pure Sciences, University of Samarra, Samarra, Iraq*

[2] *Department of Community Health, Kirkuk Technical Medical Institute, Northern Technical University, Kirkuk, Iraq*

[3] *Directorate General of Salah Uddin Education, Ministry of Education, Salah ad Din, Iraq*

[4] *College of Pharmacy, Al-Turath University, Baghdad, Iraq*

[5] *Department of Medical Laboratory Techniques, Al-Farahidi University, Baghdad, Iraq*

[6] *Department of Clinical Laboratory Sciences, College of Pharmacy, Al-Bayan University, Baghdad, Iraq*

ARTICLE INFO

Article History:
Received 27 May 2026
Accepted 18 September 2026
Published 01 October 2026

Keywords:
Chitosan
Ferroptosis
FGF21/irisin signalling
GPX4
Insulin resistance
Selenium nanoparticles

ABSTRACT

Glutathione peroxidase 4 (GPX4) is a selenoenzyme and the principal restraint upon accumulation of phospholipid hydroperoxides; its failure executes ferroptosis. Whether selenium supplied in nanoparticulate form can reinstate this restraint in insulin resistance, and whether any benefit is distinguishable from mere suppression of lipid peroxidation, has not been established. Chitosan-stabilized selenium nanoparticles (SeNPs) were synthesized by ascorbate reduction of selenious acid and characterized by TEM, DLS, zeta potential, XRD, FTIR, ICP-MS and endotoxin assay. Fifty male Wistar rats received a high-fat/high-fructose diet over 8 weeks; 48 satisfied the entry criterion and were allocated across seven groups (n = 7-8): untreated control, insulin-resistant model, model plus SeNPs 0.25 or 0.5 mg Se/kg, model plus equimolar sodium selenite, model plus ferrostatin-1, and healthy rats given SeNPs. Treatment extended from week 9 to week 14. SeNPs at 0.5 mg Se/kg reinstated hepatic GPX4 activity at 87% of control, reduced HOMA-IR by 58% (7.54 ± 2.31 to 3.15 ± 0.94), and lowered hepatic malondialdehyde and labile Fe(II). SeNPs surpassed equimolar selenite for HOMA-IR (−2.42; 95% CI −3.98 to −0.86). SeNPs and ferrostatin-1 were indistinguishable for HOMA-IR and malondialdehyde, yet ferrostatin-1 left GPX4 and SLC7A11 unaltered, dissociating selenium-dependent repair of the enzyme from blockade of peroxidation per se. Serum FGF21 declined as hepatic β-Klotho rose, and malondialdehyde mediated 49% of the GPX4–HOMA-IR relationship. The axis was characterized biochemically; ferroptotic cell death itself was not demonstrated directly.

How to cite this article
Ahmed Mustafa M, Sadiq Laylani L, M. F. Al-Samarrai M. Selenium Nanoparticles Restore GPX4 and Attenuate Ferroptosis-Associated Lipid Peroxidation While Modulating FGF21/Irisin Signalling in Insulin-Resistant Rats. J Nanostruct, 2026; 16(4):5859-5877. DOI: 10.22052/JNS.2026.04.114

* *Corresponding Author Email: mohammedahmed@uosamarra.edu.iq*

This work is licensed under the Creative Commons Attribution 4.0 International License.
To view a copy of this license, visit http://creativecommons.org/licenses/by/4.0/.

INTRODUCTION

Insulin resistance is the common prepathological state associated with the development of type 2 diabetes mellitus and clinical series always demonstrate a measurable oxidative damage. Malondialdehyde and uric acid levels were higher and glutathione levels were lower in insulin resistant patients compared to non-insulin resistant patients, and the greater the level of dyslipidaemia, the greater the concentration of malondialdehyde and uric acid, and the lower the concentration of glutathione, in Iraqi diabetic populations [1]. A separate group of Iraqi researchers found that malondialdehyde was an indirect marker for Type 2 Diabetes, through its association with triglyceride load [2]. Results like these place lipid peroxidation close to the metabolic lesion instead of in isolation, but aren't able to distinguish between its role as a cause, effect or 'incidental correlate'. Such ambiguity requires intervention at a particular target point within the peroxidation apparatus, not to oxidative stress as an overall process.

There is a node like ferroptosis. It was originally described as an iron-dependent, non-apoptotic death that occurs after erastin inhibits cystine/glutamate antiporter system xc− and depletes the antioxidant capacity in the cell [3] and is part of the regulated cell death occurring when membrane phospholipid peroxidation is not inhibited [3, 4]. The most important inhibitor is the selenoenzyme glutathione peroxidase 4 (GPX4) which uses the reducing agent glutathione to detoxify phospholipid hydroperoxides; as GPX4 decreases in activity relative to that of the hydroperoxides, propagation of the radicals occurs unchecked and cell death follows [3, 5]. The essential role of GPX4 over other antioxidant enzymes was demonstrated by chemoproteomic identification of the enzyme as direct target of a class of ferroptosis inducing compounds, whose lethality levels recapitulated the correlation of GPX4 overexpression or knockdown across twelve compounds [5] and confirmed in vivo by conditional knockout of Gpx4, which resulted in lipid-oxidation-induced renal failure and death in mice [6]. There are three more determinants which determine conditions under which this can be accomplished. Incorporation of PUFAs into phospholipids of the membrane is regulated by acyl-CoA synthetase long-chain family member 4 (ACSL4), which makes it essential in the execution of ferroptosis, as shown by the fact that Gpx4/Acsl4 double-knockout cells are almost entirely resistant [***7***] and the dependency has been confirmed in several disease contexts [6, 7]; The cystine/glutamate antiporter SLC7A11 maintains the glutathione pool required for GPX4; and the labile ferrous iron pool, replenished by the transferrin receptor 1, provides the catalytic species that converts hydroperoxides into chain-propagating radicals [3, 8].

This axis has already been described to be involved in metabolic liver disease. Based on these findings, pharmacological inhibition of ferroptosis using liproxstatin-1, which was identified in the same study that identified Gpx4 as a regulator in vivo reduced hepatic triglyceride content, measures of lipid peroxidation, and insulin resistance in diet-induced liver steatosis; iron chelation alone decreased inflammation but did not improve either lipid accumulation or insulin resistance [9]; these findings have led to the proposal that ferroptosis inhibition is a potential therapeutic strategy in metabolic dysfunction-associated fatty liver disease [10]. The point of benefit is still unknown, however. Blocking the propagation of lipid radicals and replenishing the missing enzyme, GPX4, have different mechanisms and implications and can be separated only by introducing an agent that enhances GPX4 activity, in addition to an agent that scavenges lipid radicals, which does not enhance GPX4 activity.

This comparison is possible because the catalytic selenocysteine residue of GPX4 is directly linked to the availability of selenium as a result of its catalytic activity [3, 5]. The role of selenium in metabolic disease is not however straightforwardly a deficiency. The major plasma carrier of selenium is selenoprotein P, which acts as a hepatokine that disrupts insulin signalling and glucose metabolism partly by inhibiting AMP-activated protein kinase [11] and has been postulated to create a reductive stress to modulate the physiological burst of reactive oxygen species needed for insulin signalling transductions [12]. The relative importance of chemical speciation is thus greater than elemental intake. Low doses of selenite and selenium nanoparticles (SeNPs) had opposing effects on adipose accretion and insulin signalling in adolescent rats regardless of GPX1 expression or activity [13]. However, SeNPs have been found to increase the insulin sensitivity, redox balance, and insulin-signaling protein phosphorylation in diabetic rats induced by high

CC BY

fat diet and streptozotocin [14] and in a rat model of PCOS induced by letrozole, they showed insulin-sensitizing, antioxidant, and mitochondrial effects together with PI3K/Akt pathway [15]. It's not an accidental or incidental polymer that stabilizes such particles, either. The particles studied here were stabilized with polysaccharide and polymer coatings to maintain the colloidal stability, enhance bioavailability and minimize toxicity.The ones studied here were coated with polysaccharides and polymers to achieve the following: maintain colloidal stability, enhance bioavailability, and limit toxicity, with chitosan being favored for its mucoadhesive properties, which help to lengthen residence time at the absorptive surface of the gut.

Iraqi organizations have carried out investigations which directly address both parts of this question. Here again, the nanoparticulate form of both selenium and vitamin C exerted a markedly larger protective effect than the conventional forms with respect to the oxidative, inflammatory, and apoptotic indices in gentamicin-induced injury in Wistar rats, which was concordant with the changes on Nrf2 signalling [16]. Other groups in Iraq have also synthesized selenium nanoparticles via chemical methods to the desired sizes of the particles, their surface chemistry and biological activity using UV-Vis spectroscopy, FTIR, and TEM [17]. Indeed, this is also found locally: supplementation with the trace element chromium caused significant decreases in glycated haemoglobin and fasting glucose level in Iraqi patients with poorly controlled type 2 diabetes [18] making it a practical, not a theoretical, choice for the species form of selenium delivery. In diabetic rats treated with a biogenically synthesized selenium nanoparticle, both 0.25 and 0.5 mg Se/kg have been used and shown to increase activity of glutathione peroxidase, catalase and superoxide dismutase, and to decrease the activity of liver enzymes and lipid peroxidation [19]; these same two doses were chosen in the present study. None of these works, however, tested GPX4 activity, labile iron pool, or the ferroptosis effectors, so the hypothesis that SeNPs act by re-establishing the GPX4 restraint was untested.

Two endocrine axes provide a complementary approach to ascertain if such restoration occurs with respect to systemic metabolic signalling. However, the circulating level of this hepatokine known as fibroblast growth factor 21 (FGF21) is elevated in obesity, which is considered as a state of 'FGF21 resistance' [20]. However, this interpretation is still controversial since levels of β-Klotho protein decrease during the development of diet-induced obesity in white adipocytes, and maintaining its expression in these tissues does not re-establish FGF21 signalling, suggesting that the absence of the co-receptor is not the only mechanism [21, 22]. Measurement of FGF21 in the serum, in combination with hepatic β-Klotho and FGFR1c, therefore allows for assessment of whether an intervention brings the resistant state to an end, or simply decreases the amount of the ligand. In skeletal muscle, the expression of FNDC5 is regulated by PGC-1α and irisin is produced through proteolytic processing of FNDC5; irisin is able to increase glucose uptake and mitochondrial respiration in myotubes through the p38-MAPK-PGC-1α pathway and can overcome experimentally induced insulin resistance [23, 24]. This axis is postulated to be a beneficial target of reclaimed peroxidase activity, since the transcription of FNDC5 is redox-sensitive and PGC-1α can be oxidized.

Therefore, we investigated whether the addition of chitosan-stabilized SeNPs is able to protect against GPX4-dependent ferroptosis in insulin-resistant rat hepatic and skeletal muscle tissue and if this is a measurable part of the benefit shown on insulin resistance. The experimental design is based on three discriminating comparisons: SeNPs versus equimolar sodium selenite to establish the nanoparticulate delivery effect as independent of the selenium dose per se; SeNPs versus ferrostatin-1 to establish the restoration of the enzyme effect as independent of the down stream radical interception effect; and the SeNPs when administered to healthy animals, to determine if the intervention gives rise to a safety or over-supplementation penalty. A pre-specified mediation model analysis was used to estimate the magnitude of the mediation effect of lipid peroxidation on the relationship between GPX4 activity and insulin sensitivity.

MATERIALS AND METHODS

The process of synthesizing selenium nanoparticles

Chemical reduction in an aqueous phase was used to prepare seNPs. Selenious acid was reduced with ascorbic acid as reducing agent and chitosan was added as stabilizer and capping polymer and the reaction was carried out at

(cc) BY

ambient temperature under continuous stirring until the formation of the characteristic orange-red colloidal dispersion. The preparation was dialyzed against DI water to remove any unreacted precursor and residual reducing agent, and then stored at 4 °C in light-shielding conditions. All Chemicals used were analytical grade. All the animal phase was performed with one batch of synthesis, so that the characterisation data and the data on the biological effects are related to the same material.

Characterization

Transmission electron microscopy (TEM) was used to determine the dimensions of the core and the morphology of the particles, with 118 particles manually sized. The dynamic light scattering (DLS) was combined with electrophoretic mobility measurements to determine the hydrodynamic diameter, polydispersity index, and zeta potential. X-ray diffraction (XRD) was used for assignment of crystalline phase, and Fourier-transform infrared spectroscopy (FTIR) was used for the interrogation of the surface chemistry. The total selenium content was determined in relation to the nominal concentration by ICP-MS. The colloidal stability was rechecked after 28 days of storage using DLS. The Limulus amebocyte lysate (LAL) assay method was used to estimate the endotoxin burden. The values of all the characterization parameters are given as an average of the triplicate readings made from one batch (Table 1).

Animals, housing and study timeline

Male Wistar albino rats aged 8-10 weeks and weighing 170-230 g at initial purchase were obtained from the Laboratory Animal House of the State Company for Drugs Industry and Medical Applances / Samarra, Salah Al Din Governorate, Iraq where the whole in-vivo phase were carried out. There was a 7-day acclimatization period before the start of the experiment.

Under controlled conditions, housing consisted of three to four animals per cage at the following conditions: 22 ± 2 °C, 45-65% relative humidity and a 12 h light/dark cycle. Feed and drinking water was available ad libitum, according to the feeding regimen given for each group.

The in-vivo phase began on 1st October 2024 for 14 weeks, running continuously. Week 1-8 was the induction phase, week 8 was the step for model validation and allocation and week 9-14 was the treatment phase. The following four weeks were dedicated to laboratory analysis of the samples collected and this was done in the same lab.

Diet and induction of insulin resistance

Insulin resistance was induced in male Wistar rats by means of a high-fat/high-fructose (HFHF) regimen sustained over eight consecutive weeks. The experimental feed was prepared locally within the Laboratory Animal House of the State Company for Drugs Industry and Medical Appliances / Samarra, Iraq, in accordance with the macronutrient profile of the D12492 high-fat reference formulation (Research Diets, Inc., New Brunswick, NJ, USA), which furnishes 60% of total energy as fat, 20% as protein and 20% as carbohydrate. The fat component was delivered as a mixture of beef tallow and olive oil, substituting for the lard and soybean oil employed in the reference formulation. Fructose was supplied in the drinking water at 10% w/v, corresponding to 100 g per litre of final solution. Feed and drinking water remained accessible ad libitum throughout.

At the conclusion of week 8, insulin resistance was evaluated from fasting glucose and fasting insulin concentrations determined after a 12 h fast, with HOMA-IR calculated as fasting insulin (μU/mL) x fasting glucose (mg/dL) / 405. Eligibility for the treatment phase was restricted to animals whose index attained at least twice the control group mean.

Standard laboratory chow and ordinary drinking

Table 1. Characterization of SeNPs and validation of the insulin-resistance model at week 8.
Chemical reduction produced uniform spherical particles within the pre-set acceptance limits, and 48 of 50 rats on the high-fat/high-fructose diet met the entry criterion (HOMA-IR at least twice the control mean).

Parameter	Value	Parameter	Value
TEM core size (nm), n = 118	46.8 ± 11.3 (range 27-79)	Week-8 body weight (g): chow / HFD	273 ± 19 / 331 ± 27; P < 0.001
DLS hydrodynamic size (nm) / PDI	91.2 ± 6.7 / 0.22	Fasting glucose (mg/dL)	84 ± 7 / 121 ± 15; P < 0.001
Zeta potential (mV)	−29.4 ± 3.1	Fasting insulin (μU/mL)	8.9 ± 2.1 / 21.6 ± 6.3; P < 0.001
Se content by ICP-MS (% of nominal)	94.6%	HOMA-IR	1.85 ± 0.48 / 6.47 ± 2.12; P < 0.001
DLS size stability, day 28 (% change)	+13.9%	Entry criterion / exclusions	HOMA-IR ≥ 3.70; 2 excluded (2.9 and 3.4)
LAL endotoxin (EU/mL)	0.21	Post-allocation HOMA-IR, G2-G6	6.31-6.58; ANOVA P = 0.97

XRD: trigonal Se with no selenite peaks; FTIR: chitosan bands at 1655 and 3420 cm^{-1}. Characterization values are the mean of three readings from the same batch.

CC BY

water were provided to the two chow-fed groups (G1 and G7). The HFHF regimen was sustained in groups G2-G6 throughout the treatment phase, from week 9 until the end of week 14, such that the therapeutic effects of SeNPs and of the reference treatments were assessed against ongoing metabolic stress rather than against withdrawal of the diet.

Animal accounting, entry criterion and randomization

Sixty-six male Wistar rats were employed in total. Fifty entered the eight-week high-fat/high-fructose induction regimen, while sixteen were allocated to the two chow-fed groups (G1 and G7), eight per group.

Following induction, fasting glucose and insulin were determined after a 12 h fast and HOMA-IR was calculated. The pre-specified entry criterion was a value of 3.70 or above, corresponding to twice the control group mean. Forty-eight of the fifty induced rats satisfied this criterion, two being excluded for failure to attain the threshold, with values of 2.9 and 3.4. Forty of the forty-eight qualifying animals were selected to constitute the five experimental groups G2-G6, eight per group; the eight remaining qualifying animals were retained outside the experiment and entered neither any treatment nor the final statistical analyses.

Allocation to G2-G6 proceeded by stratified randomization on week-8 HOMA-IR using a manual lottery method, so as to minimize baseline differences between groups in the severity of insulin resistance. Cages were distributed at random within the animal housing room to limit any influence of cage position, whereas direct physiological measurements were undertaken in a fixed order by group number, from G1 to G7. Baseline comparison revealed no statistically significant difference in HOMA-IR between groups G2-G6 before treatment, group means ranging from 6.31 to 6.58 ($P = 0.97$).

Experimental groups and dosing

Seven groups were investigated (n = 8 at allocation): untreated chow-fed control (G1); insulin-resistant model receiving vehicle alone (G2); model plus SeNPs 0.25 mg Se/kg (G3); model plus SeNPs 0.5 mg Se/kg (G4); model plus sodium selenite at a selenium dose equimolar to that of G4 (G5); model plus ferrostatin-1 (G6); and chow-fed healthy rats given SeNPs 0.5 mg Se/kg as a safety arm (G7).

SeNPs were delivered by oral gavage once daily at doses of 0.25 and 0.5 mg Se/kg body weight to G3 and G4 respectively, while sodium selenite was delivered to G5 by the same route at a dose equimolar in selenium to that employed in G4. Gavage volume was held constant at 5 mL/kg body weight across all groups, the concentration of active substance being adjusted to the dose assigned to each. Gavage was carried out daily at 10:00 AM over six consecutive weeks, from week 9 until the end of week 14.

Ferrostatin-1 (Fer-1; Sigma-Aldrich, catalogue number SML0583), a selective pharmacological inhibitor of ferroptosis, was administered to G6 at 2 mg/kg body weight by intraperitoneal injection once daily across the same six-week period. Fer-1 was dissolved in dimethyl sulfoxide (DMSO) and diluted in sterile physiological saline to a final concentration of 3% v/v DMSO; each solution was prepared fresh immediately prior to injection and shielded from light. An equivalent volume of the same vehicle (3% v/v DMSO in physiological saline) was given by intraperitoneal injection at identical daily frequency to all other groups (G1-G5 and G7), while G6 received an equivalent volume of the oral-treatment vehicle by gavage at the same volume and frequency, so that every group was matched for solvent exposure and for handling and injection stress. Selection of the dose rested upon an established regimen of ferrostatin-1 at 2 mg/kg in 3% v/v DMSO given by daily intraperitoneal injection over 32 consecutive days in adult male rats [25]. Fer-1 was used as a positive pharmacological control for the role of iron dependent lipid peroxidation in insulin resistance and as a comparator to SeNPs.

Humane endpoints and health monitoring

The general condition of the animals was followed twice daily during the experiment and any clinical signs or complications which were considered to be possibly related to the dietary regime or treatment were recorded early in the experimental period. The veterinary intervention was due to the presence of serious clinical symptoms; numerical thresholds for humane endpoints were not established ahead of time and this is a methodological limitation.

Two spontaneous deaths occurred during the treatment phase: one animal in the untreated

CC BY

insulin-resistant group (G2) at week 11, associated with severe hyperglycaemia, and one animal in the sodium selenite group (G5) at week 10, following an injury related to the oral gavage procedure. Neither animal was euthanized at a pre-defined endpoint. Final group sizes accordingly fell from eight to seven in G2 and G5, and neither of the two animals that died entered any of the final analyses.

Blinding and bias reduction

Blinding procedures were instituted at several stages of the experiment in order to limit the scope for bias in outcome assessment. Direct physiological measurements were obtained in a fixed, sequential order by group, from G1 to G7. Biochemical and molecular analyses, by contrast, were conducted on coded samples, the laboratory operators remaining unaware of group identity while samples were processed and analysed.

Statistical analyses were likewise conducted under blinding, group identity not being disclosed to the statistical analyst during the analysis.

Histopathological assessment of liver and kidney sections was undertaken independently by two assessors unaware of group identity or of the treatments employed. Changes were graded on a semi-quantitative 0-3 scale; inter-rater agreement proved substantial (Cohen's $\kappa = 0.81$) and disagreements were resolved by consensus between the assessors.

Adoption of a fixed order for the direct physiological measurements therefore stood in no conflict with the blinding applied to the laboratory, molecular, histological and statistical analyses.

Glucose tolerance and insulin sensitivity

An oral glucose tolerance test (2 g/kg glucose by gavage following a 12 h fast) was conducted in week 13 with sampling at 0, 15, 30, 60, 90 and 120 min; the incremental area under the glucose curve was computed by the trapezoidal rule. An insulin tolerance test followed 72 h later, the glucose disappearance constant K_ITT being derived from the slope of the natural logarithm of glucose across the linear decay phase. HOMA-β was calculated from the same fasting pair as HOMA-IR.

Anaesthesia, sample collection and euthanasia

At the end of week 14, following a 12 h fast, rats were placed under deep general anaesthesia using a combination of ketamine at 75 mg/kg body weight and xylazine at 10 mg/kg body weight administered by intraperitoneal injection. Once a surgical plane of anaesthesia had been confirmed by absence of response to noxious stimuli, blood was collected by cardiac puncture. Euthanasia was effected by exsanguination under deep anaesthesia, followed by bilateral thoracotomy as a secondary physical procedure to ensure death. Death was confirmed before any tissue was collected.

Liver, gastrocnemius muscle, epididymal adipose tissue and kidney were thereupon excised and rinsed in ice-cold physiological saline. Samples designated for biochemical and molecular analysis were snap-frozen in liquid nitrogen, whereas those designated for histology were fixed in 10% neutral buffered formalin. Serum was separated from the collected blood and stored at −80 °C.

Chemicals, kits and antibodies

Reagents for SeNP synthesis were procured from Sigma-Aldrich (Merck, Germany) and were of analytical grade: low-molecular-weight chitosan (Cat. No. 448869) as the stabilizing and capping polymer, selenious acid (Cat. No. 211176) as the selenium source, and L-ascorbic acid as the reducing agent. Ferrostatin-1 (Cat. No. SML0583) was obtained from the same supplier and prepared in DMSO and sterile physiological saline as described in section 2.6.

Enzyme-linked immunosorbent assay (ELISA) kits supplied by SunLong Biotech (China) served to determine serum insulin (Cat. No. EL1471Ra), adiponectin (Cat. No. EL0005Ra), FGF21 (Cat. No. EL1408Mt), irisin and selenoprotein P, in accordance with the manufacturer instructions.

Primary antibodies for western blotting were procured from Proteintech (USA): GPX4 (Cat. No. 67763-1-Ig), SLC7A11/xCT (Cat. No. 32384-1-AP), ACSL4 (Cat. No. 22401-1-AP), transferrin receptor 1 (TFR1/CD71, Cat. No. 81793-2-RR), ferritin heavy chain 1 (FTH1, Cat. No. 11682-1-AP), FNDC5 (Cat. No. 23995-1-AP) and Akt (Cat. No. 10176-2-AP), together with antibodies directed against phosphorylated Akt (Ser473), β-Klotho and FGFR1c. β-actin served as the internal loading reference.

Biochemical assays

Serum glucose, triglycerides, ALT, AST, ALP, urea and creatinine were determined on an automated analyser using commercial kits. Serum insulin,

CC BY

adiponectin, FGF21, irisin and selenoprotein P were determined by sandwich ELISA in duplicate. The irisin assay was cross-validated against mass spectrometry, yielding an intra-assay coefficient of variation of 9.4%. Hepatic triglycerides were extracted by the Folch method and quantified enzymatically. Hepatic superoxide dismutase, catalase and total glutathione peroxidase activities, serum total antioxidant capacity, the reduced-to-oxidized glutathione ratio, malondialdehyde and 4-hydroxynonenal were determined colorimetrically or by ELISA in tissue homogenates and normalized to protein measured by the Bradford method. Labile ferrous iron was quantified using a ferrous-selective chromogenic probe in deproteinized homogenate, and total tissue iron and selenium by ICP-MS following acid digestion.

GPX4 activity

GPX4 activity was assayed in the 100,000 × g supernatant with phosphatidylcholine hydroperoxide as substrate, which distinguishes GPX4 from the remaining glutathione peroxidases, and was monitored as the rate of NADPH consumption at 340 nm within the glutathione reductase-coupled system. Activity is expressed as nmol NADPH oxidized per minute per mg protein.

Western blotting and quantitative PCR

Proteins were resolved by SDS-PAGE, transferred onto PVDF membranes and probed with the primary antibodies listed in section 2.11. Bands were normalized to β-actin and expressed as a ratio to the G1 mean; blotting was undertaken in five animals per group. Total RNA was reverse-transcribed and *Gpx4*, *Fgf21*, *Ppargc1a* and *Ucp1* transcripts were quantified by real-time PCR, expression being normalized to the geometric mean of *Actb* and *Hprt1* and reported as fold change relative to G1.

Histopathology

Formalin-fixed, paraffin-embedded liver and kidney sections were stained with haematoxylin and eosin and graded as described in section 2.8.

Statistical analysis

The individual animal constituted the experimental unit for every outcome, and all analyses were conducted at the animal level. HOMA-IR at week 14 was the primary outcome; hepatic GPX4 activity and hepatic malondialdehyde were pre-specified co-primary mechanistic outcomes. All remaining measures were secondary and exploratory and are reported as such. The two animals that died during the treatment phase were handled by complete-case analysis; no values were imputed, and the reduced group sizes (n = 7 for G2 and G5) are carried through every affected result, yielding 54 animals in the final analyses.

Analyses were conducted in IBM SPSS Statistics version 26 (IBM Corp., Armonk, NY, USA). Normality was evaluated by the Shapiro-Wilk test. Normally distributed variables are reported as mean ± standard deviation and compared by one-way ANOVA followed by Tukey HSD; variables failing normality ($P < 0.05$) are reported as median [interquartile range] and compared by the Kruskal-Wallis test followed by the Dunn test. Homogeneity of variance was examined for every normally distributed outcome by the Levene test, supported by inspection of the ratio of the largest to the smallest group variance. Where that assumption was not met, the omnibus test was repeated as a Welch ANOVA and the exploratory all-pairs comparisons as the Games-Howell procedure [26, 27], which assume neither equal variances nor equal group sizes; results obtained under the two approaches are compared in section 3.9. Omnibus P values across the seven groups were corrected for multiple testing by the Benjamini-Hochberg procedure [28] and are reported as q values. The OGTT time course was analysed by repeated-measures ANOVA incorporating a group × time interaction.

Five contrasts were specified in advance, before any between-group comparison had been examined: G2 versus G1 (model validity), G4 versus G2 (principal effect), G4 versus G5 (nanoparticulate versus inorganic selenium), G4 versus G6 (mechanistic equivalence to a ferroptosis inhibitor) and G7 versus G1 (safety). These were Holm-corrected and are reported as mean differences with 95% confidence intervals and Cohen's d. Associations within the pooled high-fat groups (G2-G6, n = 38) were examined by Spearman rank correlation. Mediation along the GPX4 activity to malondialdehyde to HOMA-IR pathway was tested using a single-mediator model (PROCESS model 4) [29] with 5000 bootstrap resamples, and a sensitivity analysis repeated the model with final body weight as a covariate.

CC BY

Because the five contrasts were specified in advance, they were tested as Welch t contrasts (which do not assume equal variances) with Holm correction [30] applied across the five, rather than by an all-pairs post-hoc procedure. Two-sided P < 0.05 was taken as significant. Group size was not fixed by an a priori power calculation; a sensitivity analysis establishing the smallest effect the design could detect is reported in section 3.9.

Ethical approval

The Scientific Research Ethics Committee of the College of Education for Pure Sciences, University of Samarra, gave approval to the experimental protocol, with reference number EDUSamaraH01 Bio-9 dated 1 October 2024. All procedures conducted with laboratory animals were performed in accordance with institutional guidelines for the care and use of laboratory

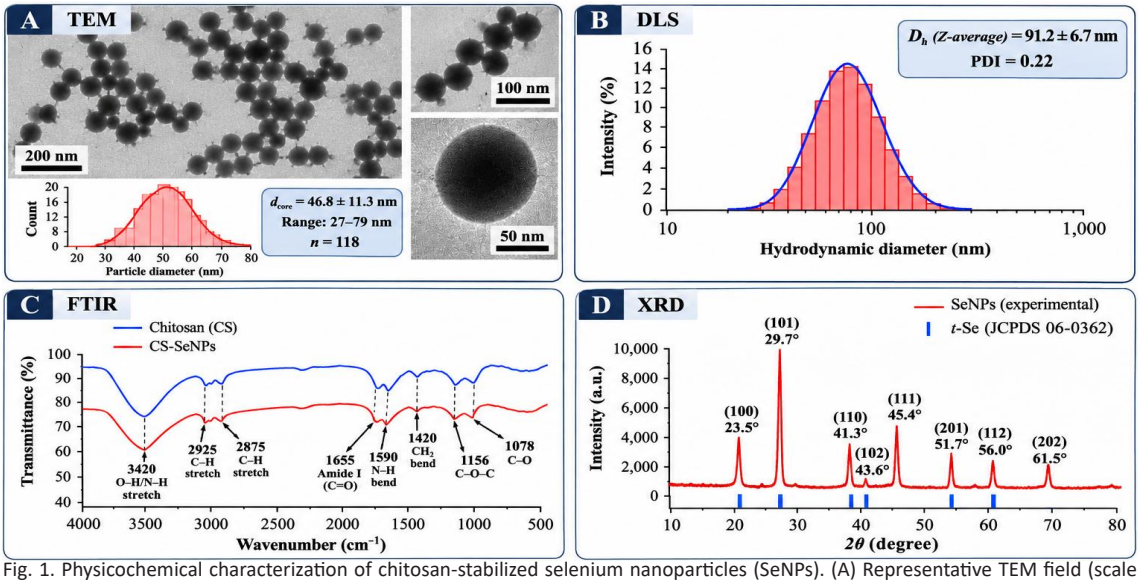


Fig. 1. Physicochemical characterization of chitosan-stabilized selenium nanoparticles (SeNPs). (A) Representative TEM field (scale bar: 200 nm); right-hand panels, higher-magnification views (scale bars: 100 and 50 nm). The particle core diameter averaged 46.8 ± 11.3 nm (range: 27–79 nm) over 118 manually measured particles; the inset shows the corresponding size distribution (red line, Gaussian fit). (B) Intensity-weighted hydrodynamic size distribution by DLS (D_h = 91.2 ± 6.7 nm; PDI = 0.22). (C) FTIR spectra of chitosan (CS) and CS-SeNPs, showing characteristic bands at 3420 cm^{-1} (O–H/N–H stretch), 2925 and 2875 cm^{-1} (C–H stretches), 1655 cm^{-1} (amide I, C=O), 1590 cm^{-1} (N–H bend), 1420 cm^{-1} (CH_2 bend), 1156 cm^{-1} (C–O–C) and 1078 cm^{-1} (C–O). (D) XRD pattern indexed to trigonal elemental selenium (JCPDS 06-0362) with reflections at 2θ = 23.5° (100), 29.7° (101), 41.3° (110), 43.6° (102), 45.4° (111), 51.7° (201), 56.0° (112) and 61.5° (202), with no reflections attributable to selenite. Except for TEM (n = 118), values are the mean of three readings from a single synthesis batch (Table 1).

Table 2. Metabolic phenotype and insulin sensitivity at the end of week 14.
SeNPs at 0.5 mg/kg lowered HOMA-IR by 58% relative to the model, approaching ferrostatin-1 and exceeding equimolar sodium selenite; the low dose improved glucose and the OGTT without reaching significance for HOMA-IR against the model.

Variable	G1 Control (n=8)	G2 IR (n=7)	G3 IR+SeNPs 0.25 (n=8)	G4 IR+SeNPs 0.5 (n=8)	G5 IR+selenite (n=7)	G6 IR+Fer-1 (n=8)	G7 Healthy+SeNPs (n=8)	P (ANOVA/KW)
Final body weight (g)	327 ± 21	409 ± 31 a	384 ± 28 a	362 ± 24 ab	391 ± 33 a	371 ± 26 ab	319 ± 19	< 0.001
Fasting glucose (mg/dL)	86 ± 8	134 ± 17 a	114 ± 13 ab	101 ± 11 bc	119 ± 14 a	104 ± 12 b	83 ± 9	< 0.001
Fasting insulin (µU/mL)	9.2 ± 2.4	22.7 ± 6.1 a	17.9 ± 4.8 a	12.6 ± 3.3 bc	18.8 ± 5.6 a	13.4 ± 3.9 b	8.7 ± 2.0	< 0.001
HOMA-IR	1.96 ± 0.58	7.54 ± 2.31 a	5.08 ± 1.62 a	3.15 ± 0.94 bc	5.57 ± 1.88 a	3.46 ± 1.12 b	1.79 ± 0.47	< 0.001
HOMA-β (%)	141 ± 36	98 ± 29 a	126 ± 34	138 ± 31 b	112 ± 33	129 ± 30	149 ± 38	0.004
OGTT area (mg·min/dL ×10^3)	14.3 ± 1.6	23.9 ± 3.1 a	19.6 ± 2.4 ab	16.8 ± 2.0 bc	20.7 ± 2.8 a	17.1 ± 2.2 b	13.9 ± 1.5	< 0.001
K_ITT (%/min)	4.41 ± 0.72	2.03 ± 0.49 a	2.84 ± 0.61 a	3.72 ± 0.68 bc	2.61 ± 0.58 a	3.49 ± 0.66 b	4.52 ± 0.81	< 0.001
Serum triglycerides (mg/dL)	61 [52-74]	139 [112-168] a	108 [89-131] a	84 [70-103] bc	117 [96-142] a	96 [78-118] b	58 [49-71]	< 0.001
Hepatic triglycerides (mg/g)	13.1 ± 3.4	44.7 ± 11.2 a	33.6 ± 9.1 a	22.4 ± 6.3 bc	36.9 ± 10.4 a	26.1 ± 7.5 b	12.4 ± 3.1	< 0.001
Adiponectin (µg/mL)	8.3 ± 1.9	4.6 ± 1.3 a	5.9 ± 1.6 a	7.2 ± 1.8 b	5.4 ± 1.5 a	6.8 ± 1.7 b	8.6 ± 2.0	< 0.001
Muscle p-Akt(Ser473)/Akt (ratio to G1)	1.00 ± 0.21	0.47 ± 0.14 a	0.69 ± 0.18 a	0.88 ± 0.20 bc	0.61 ± 0.17 a	0.83 ± 0.19 b	0.97 ± 0.22	< 0.001

Mean ± SD, or median [IQR] for non-normal variables (Shapiro-Wilk P < 0.05). One rat died in G2 (week 11, severe hyperglycaemia) and one in G5 (week 10, gavage-related injury). One-way ANOVA then Tukey HSD, or Kruskal-Wallis then Dunn; a: P < 0.05 vs G1; b: vs G2; c: vs G5; P values shown are Benjamini-Hochberg corrected (q). Western blot n = 5/group. OGTT: RM-ANOVA group × time P < 0.001. G3 vs G2 for HOMA-IR: P = 0.11.

CC BY

animals and in compliance with internationally agreed upon guidelines for animal welfare. To minimize the distress of animals, to limit the number of animals used, and to ensure proper housing, handling, and veterinary care throughout the experiment, steps were taken. Before entry of the first animal the study protocol was presented to and approved by the committee above, but not submitted to nor published in any public protocol repository, and the pre-specified contrasts were not included. This manuscript has been written according to ARRIVE 2.0 guidelines.

RESULTS AND DISCUSSION

Tables 1–6 are provided as separate documents along with the narrative and are not repeated.

All the spherical particles were chemically reduced and they were found to be within the limits of acceptance, defined a priori (Table 1). The core diameter obtained by TEM analysis was 46.8 ± 11.3 nm (range from 27 nm to 79 nm) and the hydrodynamic diameter was 91.2 ± 6.7 nm with a polydispersity index of 0.22, which could have been caused by the small hydration and chitosan shell and not by aggregation of particles. The zeta potential of −29.4 ± 3.1 mV is consistent with an electrostatically stabilized colloidal system, and there was almost no change in hydrodynamic diameter after storage for 28 days (maximum 13.9%). ICP-MS gave a selenium content of 94.6% of the nominal, resulting in delivered dose being very close to the intended dose. The XRD patterns showed no peaks of selenite, meaning that all the selenium was reduced to trigonal elemental selenium, whereas the FTIR patterns showed the characteristic chitosan bands at 1655 and 3420

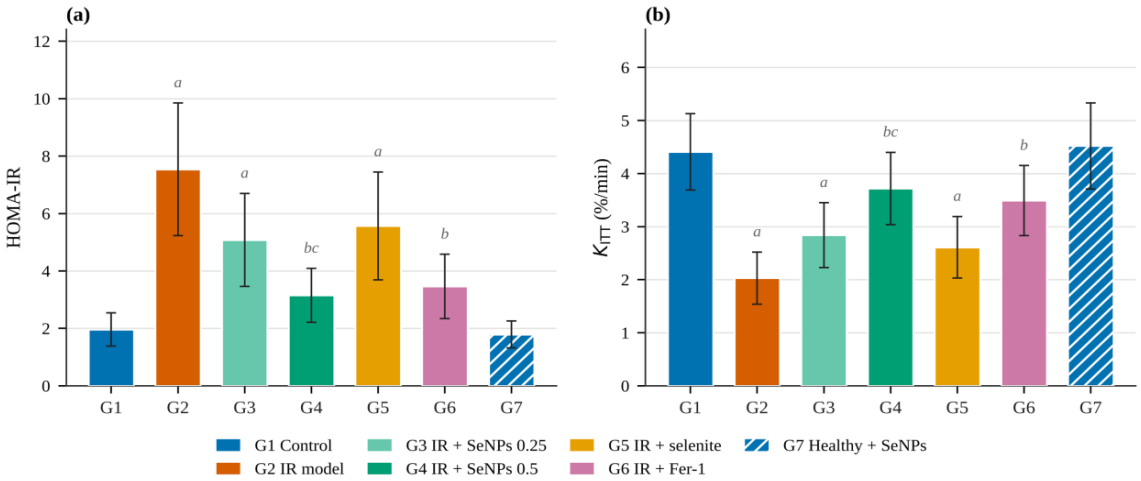


Fig. 2. The insulin sensitivity for each of the seven experimental groups after 14 weeks. (a) HOMA-IR; (b) the glucose disappearance constant K_ITT. Bars show mean ± SD (n = 8 per group; n = 7 in G2 and G5). One-way ANOVA and Tukey HSD; a: P < 0.05 compared to G1; b: compared to G2; c: compared to G5. The reduction in HOMA-IR compared to the model was 58% in SeNPs 0.5 mg Se/kg (G4) and not different from FeS (G6) while equimolar Se (G5) was not different from the model.

Table 3. The FGF21/β-Klotho and irisin/FNDC5 axes.
The fall in serum FGF21 after SeNPs was accompanied by a rise in hepatic β-Klotho, consistent with easing of FGF21 resistance; serum irisin rose only at the higher dose and remained highly variable, while the change in adipose Ucp1 was not significant after correction.

Variable	G1 Control (n=8)	G2 IR (n=7)	G3 IR+SeNPs 0.25 (n=8)	G4 IR+SeNPs 0.5 (n=8)	G5 IR+selenite (n=7)	G6 IR+Fer-1 (n=8)	G7 Healthy+SeNPs (n=8)	P (ANOVA/KW)
Serum FGF21 (pg/mL)	203 [158-261]	587 [421-794] a	446 [338-602] a	312 [231-418] ab	503 [372-671] a	351 [264-466] ab	219 [171-284]	< 0.001
Hepatic Fgf21 mRNA (fold change)	1.00 ± 0.34	3.12 ± 1.08 a	2.37 ± 0.86 a	1.71 ± 0.62 b	2.58 ± 0.94 a	1.89 ± 0.71 b	1.13 ± 0.39	< 0.001
Hepatic β-Klotho (protein, ratio)	1.00 ± 0.19	0.52 ± 0.15 a	0.68 ± 0.17 a	0.84 ± 0.18 b	0.63 ± 0.16 a	0.77 ± 0.19 b	0.96 ± 0.21	< 0.001
Hepatic FGFR1c (protein, ratio)	1.00 ± 0.22	0.71 ± 0.18 a	0.79 ± 0.20	0.91 ± 0.21	0.74 ± 0.19 a	0.86 ± 0.20	1.04 ± 0.24	0.021
Serum irisin (ng/mL)	11.9 ± 3.6	7.1 ± 2.4 a	8.6 ± 2.9	10.4 ± 3.1 b	8.0 ± 2.7 a	9.7 ± 3.0	12.3 ± 3.8	0.003
Muscle FNDC5 (protein, ratio)	1.00 ± 0.23	0.49 ± 0.16 a	0.66 ± 0.19 a	0.85 ± 0.21 b	0.58 ± 0.17 a	0.78 ± 0.20 b	1.02 ± 0.25	< 0.001
Muscle Ppargc1a mRNA (fold change)	1.00 ± 0.31	0.51 ± 0.19 a	0.69 ± 0.24 a	0.86 ± 0.27 b	0.62 ± 0.22 a	0.81 ± 0.26 b	1.08 ± 0.33	< 0.001
Adipose Ucp1 (fold change)	1.00 ± 0.42	0.63 ± 0.29	0.81 ± 0.36	1.09 ± 0.44	0.72 ± 0.33	0.94 ± 0.39	1.17 ± 0.48	0.083

Mean ± SD, or median [IQR] for non-normal variables. Statistical annotations as in Table 2. Irisin measured with an ELISA cross-validated by mass spectrometry (intra-assay CV 9.4%); mRNA normalized to the geometric mean of Actb and Hprt1. Correlation of serum FGF21 with hepatic β-Klotho: r = −0.58, P < 0.001 (n = 54).

CC BY

cm^{-1}, which were consistent with the expected results. Endotoxin was not high enough to contribute to the biological responses seen and was 0.21 EU/mL (Fig. 1).

Performance of the dietary model conformed to expectation. At week 8, the body weight of the high-fat/high-fructose group was 331 ± 27 g versus 273 ± 19 g for the controls, and fasting glucose was 121 ± 15 versus 84 ± 7 mg/dL and fasting insulin was 21.6 ± 6.3 versus 8.9 ± 2.1 µU/mL (P < 0.001 throughout). A rise in HOMA-IR from 1.85 ± 0.48 to 6.47 ± 2.12 accompanied these changes. Forty-eight of the fifty induced rats met the entry requirement of 3.70, two were just below that and were excluded; forty animals were placed into G2–G6 and eight were kept outside of the experiment. Stratified allocation ensured baseline equivalence by treatment group (G2–G6, 6.31–6.58; P = 0.97) and allowed any differences in the week-14 outcomes to be attributed to treatment rather than to differences in baseline severity.

Metabolic phenotype and insulin sensitivity

At study termination, HOMA-IR in the untreated model group stood at 7.54 ± 2.31 as against 1.96 ± 0.58 in controls (Table 2; Fig. 2a). Administration of SeNPs at 0.5 mg Se/kg brought HOMA-IR down to 3.15 ± 0.94 — a 58% reduction with respect to the model — and this improvement proved internally consistent across each independent

Table 4. The GPX4-dependent ferroptosis axis in liver and skeletal muscle.
High-dose SeNPs restored hepatic GPX4 activity to 87% of the control value and reduced labile iron and lipid peroxidation to an extent comparable with ferrostatin-1, whereas ferrostatin-1 lowered lipid peroxidation without altering GPX4 or SLC7A11 - separating the effect of selenium on the enzyme from suppression of peroxidation per se.

(a) Liver

Variable	G1 Control (n=8)	G2 IR (n=7)	G3 IR+SeNPs 0.25 (n=8)	G4 IR+SeNPs 0.5 (n=8)	G5 IR+selenite (n=7)	G6 IR+Fer-1 (n=8)	G7 Healthy+SeNPs (n=8)	P (ANOVA/KW)
GPX4 activity (nmol NADPH/min/mg)	26.3 ± 5.1	11.8 ± 3.6 a	17.2 ± 4.4 a	22.9 ± 4.8 bc	15.1 ± 4.1 a	12.6 ± 3.9 a	30.7 ± 6.2	< 0.001
GPX4 protein (ratio)	1.00 ± 0.24	0.43 ± 0.15 a	0.68 ± 0.19 a	0.89 ± 0.22 bc	0.59 ± 0.17 a	0.47 ± 0.16 a	1.14 ± 0.27	< 0.001
Gpx4 mRNA (fold change)	1.00 ± 0.29	0.56 ± 0.21 a	0.74 ± 0.25	0.93 ± 0.28 b	0.67 ± 0.23 a	0.61 ± 0.22 a	1.19 ± 0.34	0.002
SLC7A11/xCT (protein, ratio)	1.00 ± 0.22	0.54 ± 0.17 a	0.71 ± 0.19 a	0.88 ± 0.21 b	0.66 ± 0.18 a	0.62 ± 0.19 a	1.03 ± 0.24	< 0.001
ACSL4 (protein, ratio)	1.00 ± 0.26	2.41 ± 0.68 a	1.83 ± 0.54 a	1.37 ± 0.41 b	1.96 ± 0.59 a	1.44 ± 0.46 b	0.93 ± 0.25	< 0.001
TfR1 (protein, ratio)	1.00 ± 0.27	1.92 ± 0.61 a	1.58 ± 0.49	1.29 ± 0.42 b	1.66 ± 0.53 a	1.51 ± 0.47	0.97 ± 0.28	0.006
GSH/GSSG	10.6 ± 2.8	4.7 ± 1.6 a	6.9 ± 2.1 a	9.1 ± 2.5 b	6.1 ± 1.9 a	6.4 ± 2.0 a	11.3 ± 3.1	< 0.001
MDA (nmol/mg protein)	1.91 ± 0.47	4.86 ± 1.23 a	3.52 ± 0.94 a	2.47 ± 0.68 bc	3.94 ± 1.06 a	2.61 ± 0.74 b	1.78 ± 0.44	< 0.001
4-HNE (ng/mg protein)	13.6 [10.2-17.9]	34.8 [26.1-46.3] a	25.4 [18.9-33.7] a	17.9 [13.4-23.8] bc	28.7 [21.3-38.2] a	18.6 [14.1-24.9] b	12.8 [9.7-16.8]	< 0.001
Labile Fe(II) (nmol/mg protein)	0.91 ± 0.26	2.17 ± 0.63 a	1.68 ± 0.51 a	1.21 ± 0.38 b	1.84 ± 0.57 a	1.26 ± 0.41 b	0.86 ± 0.24	< 0.001
Total iron (µg/g)	124 ± 27	211 ± 54 a	178 ± 46 a	149 ± 38 b	189 ± 51 a	156 ± 41 b	118 ± 25	< 0.001
Ferritin FTH1 (ratio)	1.00 ± 0.25	0.61 ± 0.19 a	0.76 ± 0.21	0.89 ± 0.23 b	0.69 ± 0.20 a	0.84 ± 0.22	1.02 ± 0.26	0.009

(b) Gastrocnemius muscle

Variable	G1 Control (n=8)	G2 IR (n=7)	G3 IR+SeNPs 0.25 (n=8)	G4 IR+SeNPs 0.5 (n=8)	G5 IR+selenite (n=7)	G6 IR+Fer-1 (n=8)	G7 Healthy+SeNPs (n=8)	P (ANOVA/KW)
GPX4 activity (nmol/min/mg)	18.4 ± 4.2	9.3 ± 2.9 a	12.7 ± 3.6 a	16.1 ± 4.0 b	11.2 ± 3.3 a	9.9 ± 3.1 a	21.6 ± 5.0	< 0.001
ACSL4 (protein, ratio)	1.00 ± 0.24	2.04 ± 0.58 a	1.61 ± 0.47 a	1.28 ± 0.39 b	1.73 ± 0.52 a	1.35 ± 0.42 b	0.96 ± 0.23	< 0.001
MDA (nmol/mg protein)	1.52 ± 0.39	3.61 ± 0.97 a	2.74 ± 0.78 a	2.03 ± 0.61 b	2.98 ± 0.84 a	2.12 ± 0.63 b	1.47 ± 0.36	< 0.001
Labile Fe(II) (nmol/mg protein)	0.49 ± 0.15	1.07 ± 0.32 a	0.86 ± 0.27 a	0.63 ± 0.21 b	0.92 ± 0.29 a	0.66 ± 0.22 b	0.47 ± 0.14	< 0.001

Mean ± SD, or median [IQR] for non-normal variables. Statistical annotations as in Table 2. GPX4 activity assayed with phosphatidylcholine hydroperoxide as substrate. G4 vs G6: GPX4 activity P < 0.001, MDA P = 0.71, Fe(II) P = 0.82. G7 vs G1: GPX4 activity P = 0.038; all other markers P > 0.3.

Table 5. Antioxidant enzymes, selenium status and safety markers.
SeNPs raised hepatic selenium and selenoprotein P above the equimolar selenite arm and normalized ALT and AST, whereas selenite was associated with a smaller improvement and persistently elevated ALT; safety markers in G7 did not differ from control.

Variable	G1 Control (n=8)	G2 IR (n=7)	G3 IR+SeNPs 0.25 (n=8)	G4 IR+SeNPs 0.5 (n=8)	G5 IR+selenite (n=7)	G6 IR+Fer-1 (n=8)	G7 Healthy+SeNPs (n=8)	P (ANOVA/KW)
Hepatic SOD (U/mg protein)	47.2 ± 9.6	28.4 ± 7.1 a	36.1 ± 8.3 a	42.6 ± 9.0 b	33.7 ± 8.0 a	34.9 ± 8.4 a	48.9 ± 10.1	< 0.001
Hepatic CAT (U/mg protein)	59.8 ± 12.4	34.6 ± 9.2 a	45.3 ± 10.6 a	53.1 ± 11.5 b	42.8 ± 10.1 a	43.6 ± 10.4 a	61.2 ± 13.0	< 0.001
Hepatic total GPx (U/mg protein)	112 ± 24	63 ± 18 a	94 ± 22 b	121 ± 26 bc	88 ± 21 a	69 ± 19 a	131 ± 29	< 0.001
Serum TAC (mmol/L)	1.38 ± 0.29	0.79 ± 0.21 a	1.04 ± 0.25 a	1.26 ± 0.27 b	0.98 ± 0.24 a	1.01 ± 0.25 a	1.44 ± 0.31	< 0.001
Hepatic Se (µg/g)	0.79 ± 0.14	0.66 ± 0.13	0.98 ± 0.18 ab	1.31 ± 0.23 abc	1.04 ± 0.19 ab	0.68 ± 0.14	1.36 ± 0.25 a	< 0.001
Serum selenoprotein P (µg/mL)	2.71 ± 0.54	2.08 ± 0.46 a	2.63 ± 0.52 b	3.14 ± 0.61 bc	2.69 ± 0.55 b	2.11 ± 0.48 a	3.22 ± 0.66 a	< 0.001
ALT (U/L)	36 ± 8	71 ± 19 a	54 ± 14 a	43 ± 11 b	62 ± 17 a	49 ± 13 b	38 ± 9	< 0.001
AST (U/L)	87 ± 16	147 ± 34 a	116 ± 27 a	98 ± 22 b	126 ± 31 a	104 ± 24 b	89 ± 18	< 0.001
ALP (U/L)	152 ± 31	208 ± 47 a	184 ± 41	167 ± 36	193 ± 44	176 ± 39	155 ± 33	0.034
Urea (mg/dL)	39 ± 7	47 ± 9	44 ± 8	41 ± 7	46 ± 9	43 ± 8	40 ± 7	0.19
Creatinine (mg/dL)	0.57 ± 0.09	0.66 ± 0.12	0.62 ± 0.11	0.59 ± 0.10	0.65 ± 0.12	0.61 ± 0.10	0.58 ± 0.09	0.27
Liver H&E: steatosis (0-3)	0 [0-0]	2 [2-3] a	2 [1-2] a	1 [0-1] b	2 [1-2] a	1 [1-2] b	0 [0-0]	< 0.001
Kidney H&E: tubular change (0-3)	0 [0-0]	1 [0-1]	0 [0-1]	0 [0-0]	1 [0-1]	0 [0-1]	0 [0-0]	0.14

Mean ± SD, or median [IQR] for non-normal variables. Statistical annotations as in Table 2. Se measured by ICP-MS; H&E scores assigned blinded (inter-rater κ = 0.81). ALT in G5 vs G4: P = 0.047.

CC BY

index of insulin action: fasting insulin declined to 12.6 ± 3.3 µU/mL, the OGTT area to 16.8 ± 2.0 ×10³ mg·min/dL, K_ITT increased to 3.72 ± 0.68 %/min (Fig. 2b), and the muscle p-Akt(Ser473)/Akt ratio was restored to 0.88 ± 0.20 of the control value from 0.47 ± 0.14 in the model. HOMA-β moved concurrently in the same direction (138 ± 31% versus 98 ± 29%), although the omnibus test for this index did not survive the Welch analysis (P = 0.13); it is reported as evidence that the benefit was not obtained at the cost of β-cell output, not as an independent effect.

The low dose produced a partial rather than a null effect. SeNPs at 0.25 mg/kg improved fasting glucose (114 ± 13 mg/dL) and the OGTT area (19.6 ± 2.4 ×10³), yet the difference in HOMA-IR from the model failed to attain significance (5.08 ± 1.62; P = 0.11), situating the threshold for a reliable insulin-sensitizing effect between the two doses.

Equimolar selenite proved consistently weaker than the nanoparticulate form. G5 remained statistically indistinguishable from the model with respect to HOMA-IR, fasting insulin, K_ITT and p-Akt, whereas the high SeNP dose differed from both. Hepatic triglycerides declined from 44.7 ± 11.2 to 22.4 ± 6.3 mg/g under SeNPs 0.5 mg/kg as against 36.9 ± 10.4 mg/g under selenite, while serum adiponectin rose to 7.2 ± 1.8 µg/mL as against 5.4 ± 1.5. Ferrostatin-1 yielded an insulin-sensitivity profile approaching that of the high SeNP dose. Healthy animals given SeNPs (G7) were indistinguishable from controls across every metabolic measure.

The superiority of SeNPs over equimolar sodium selenite is not attributable to selenium dose, which was matched. Two observations narrow the explanation. First, hepatic selenium and serum selenoprotein P were higher in the SeNP arm than in the selenite arm (Table 5), indicating that delivery to the tissue of interest differed. Second, ALT remained elevated under selenite while normalizing under SeNPs, consistent with the narrow therapeutic window of inorganic selenium salts, which undergo redox cycling with oxygen and cellular thiols on reduction to selenide, generating superoxide non-stoichiometrically [31]. Divergence of this kind by chemical form has precedent: in adolescent rats, low-dose selenite and SeNPs produced opposite effects upon white adipose deposition and upon insulin signalling, and those effects proved independent of GPX1 expression or activity, indicating that the two forms are not interchangeable even at equal elemental doses [13].

The GPX4-dependent ferroptosis axis

Hepatic GPX4 activity was reduced by half in the model (11.8 ± 3.6 versus 26.3 ± 5.1 nmol NADPH/min/mg), accompanied by a decline in GPX4 protein to 0.43 ± 0.15 of control; the corresponding reduction at transcript level was more modest (0.56 ± 0.21-fold), signifying that the loss of catalytic activity was not of purely transcriptional origin (Table 4; Fig. 3a). Treatment with SeNPs at 0.5 mg/kg restored activity to 22.9 ± 4.8 — 87% of the control value — with protein at 0.89 ± 0.22 and *Gpx4* transcript at 0.93 ± 0.28-fold. Recovery of SLC7A11/xCT reached 0.88 ± 0.21 of control, ACSL4 decreased from 2.41 ± 0.68 to 1.37 ± 0.41, and transferrin receptor 1 fell while ferritin heavy chain 1 increased — a pairing indicative of diminished iron import alongside enhanced iron sequestration. Both are western-blot outcomes measured in five animals per group, and neither omnibus test survived the Welch analysis (P = 0.054 and P = 0.16); they are therefore reported as a directionally coherent pattern rather than as individually established effects.

Indices downstream followed the trends upstream. The GSH/GSSG ratio increased from 4.7 ± 1.6 to 9.1 ± 2.5; malondialdehyde decreased from 4.86 ± 1.23 to 2.47 ± 0.68 nmol/mg protein, 4-hydroxynonenal from 34.8 [26.1–46.3] to 17.9 [13.4–23.8] ng/mg, labile Fe(II) from 2.17 ± 0.63 to 1.21 ± 0.38 nmol/mg, and total hepatic iron from 211 ± 54 to 149 ± 38 µg/g (Fig. 3b, c). This equivalent profile was seen in gastrocnemius muscle, where GPX4 activity was restored from 9.3 ± 2.9 to 16.1 ± 4.0 nmol/min/mg and there was a corresponding decrease in ACSL4, malondialdehyde and labile iron; showing that the effect was not limited to hepatic tissue. The muscle changes reported here are not simply an extension of the hepatic one, as ferroptosis has been described in a variety of skeletal-muscle diseases, with iron deposition and loss of GPX4 and a decrease in functional capacity [28].

The most informative finding in the dataset is the comparison of G4 with G6 and is mechanistically decisive (Fig. 3). Hepatic malondialdehyde was reduced by Ferrostatin-1 to 2.61 ± 0.74 which was not significantly different from that of the high dose of SeNP (2.61 ± 0.74) (P = 0.71), GPX4 activity was 12.6 ± 3.9, GPX4 protein 0.47 ± 0.16,

CC BY

and SLC7A11 was 0.62 ± 0.19 (all not significantly different from the model G4 versus G6, with P < 0.001 for all). Two interventions came together by two different pathways to the same peroxidation endpoint – one restoring the enzyme, the other intercepting the lipid radicals downstream. This pharmacology can be expected and is supported by the fact that the antioxidant properties of ferrostatin-1 result in the termination of the propagation phase of lipid peroxidation without restoring peroxidases activity, whereas GPX4 activity depends on availability of its catalytic selenocysteine, and therefore on selenium supply [3, 5].

It is logical in this model that metabolic benefits obtained by inhibiting ferroptosis do not require the re-activation of the enzyme—arresting the chain reaction downstream reaches the same endpoint of insulin-sensitivity. The benefit of enzyme restoration is that it is a capacity—not interception—restoration. The 87% GPX4 activity in a tissue is sufficient to neutralize the hydroperoxides as they are formed, a process which cannot be performed by a radical trap once removed. Those two mechanisms make a difference when it comes to translation: the durability after withdrawal from the treatment should be where they should be different, but the present design, which doesn't include a washout, doesn't allow for that. The accompanying changes in the ACSL4, transferrin receptor 1, and ferritin heavy chain 1 indicate that SeNPs also altered the substrate and catalyst arms of the reaction and not just the detoxifying arm. ACSL4 regulates the incorporation of polyunsaturated acyl chains into membrane phospholipids and is a known cell death regulator for ferroptosis, which is activated with the upregulation of transferrin receptor 1 in cells that are vulnerable to ferroptosis [6, 7]. These data do not allow us to distinguish whether these observations are a direct effect of selenoprotein-dependent redox signalling on the expression of ACSL4, or rather a secondary effect of reduced hepatic lipid flux. Those two should be complemented with a third. ACSL4 is not only a determinant of ferroptosis sensitivity but also a regulator of fatty-acid metabolism as the protein abundance of ACSL4 in diabetic liver can be regulated by post-translation mechanisms: ACSL4 protein is degraded by the autophagy-lysosome pathway, and inhibition of autophagic flux increases protein abundance of ACSL4 and promotes hepatocyte ferroptosis in both streptozotocin-diabetic rats and in palmitate-treated hepatocytes [30]. If ACSL4 protein was found to be decreased but no change in transcription was detected, this could be due to a restoration of ACSL4 degradation, and the present design was not able to rule this out as a cause of the decrease in ACSL4 protein.

In healthy animals there was no difference in any of the other markers, but GPX4 activity was

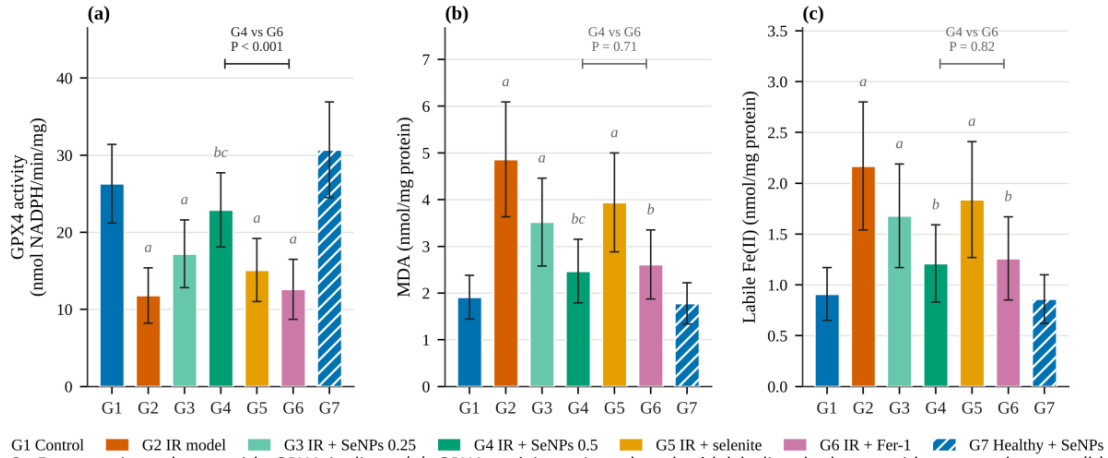


Fig. 3. Ferroptosis pathway with GPX4 in liver. (a) GPX4 activity using phosphatidylcholine hydroperoxide as a substrate; (b) malondialdehyde; (c) labile Fe(II). Data are represented as mean ± SD (bars) or as statistical annotations as in Figure 2. The brackets mark the mechanistically decisive contrast: SeNPs 0.5 mg Se/kg (G4) and ferrostatin-1 (G6) reached the same peroxidation and labile-iron endpoints (P = 0.71 and P = 0.82) yet differed sharply in GPX4 activity (P < 0.001), separating repair of the enzyme from interception of lipid radicals downstream of it.

CC BY

numerically greater in the SeNP arm (30.7 ± 6.2 versus 26.3 ± 5.1, all P > 0.3). This difference was nominally significant under the equa-lvariance analysis (P = 0.038), but failed the Welch contrast analysis (P = 0.14) and is therefore not considered to be a confirmed effect here. The present study, however, does not address the upper bound of the dose–response relationship, which is represented in the present numerical excess.

Antioxidant enzymes, selenium status and safety

SeNPs elevated hepatic selenium to 1.31 ± 0.23 μg/g and serum selenoprotein P to 3.14 ± 0.61 μg/mL, both exceeding the equimolar selenite group (1.04 ± 0.19 μg/g and 2.69 ± 0.55 μg/mL) and thereby indicating greater bioavailability at the same selenium dose rather than a difference in dose (Table 5). Total hepatic GPx activity, superoxide dismutase, catalase and serum total antioxidant capacity all improved in a dose-ordered manner, and the low SeNP dose sufficed to raise total GPx significantly above the model notwithstanding its failure to alter HOMA-IR significantly.

Safety markers favoured the nanoparticulate form. ALT normalized under SeNPs 0.5 mg/kg (43 ± 11 U/L as against 36 ± 8 in controls) but remained elevated under selenite (62 ± 17 U/L; G5 versus G4 P = 0.047), and AST followed the same ordering. Urea, creatinine and renal tubular histology did not differ across groups (P = 0.19, 0.27 and 0.14), while hepatic steatosis grade declined from 2 [2-3] in the model to 1 [0-1] under the high SeNP dose. The healthy SeNP arm matched controls on every safety variable. The same property that makes the nanoparticulate form more bioavailable is also the one that warrants caution at higher doses: uncontrolled penetration of selenium nanoparticles across cellular membranes has been raised as a potential liability precisely because it bypasses the regulated handling that inorganic salts undergo [32].

The rise in selenoprotein P warrants comment, since the broader selenium-diabetes literature counsels caution against interpreting any increase in selenium status as benign. Selenoprotein P is a hepatokine that compromises insulin signalling and glucose metabolism partly through AMPK inactivation [33], and has been argued to induce a reductive stress suppressing the physiological reactive-oxygen-species burst required for insulin signal transduction, which may account for the association between selenium supplementation and increased diabetes risk reported in intervention studies [34]. In this study, SeNP increased together with increased, not decreased insulin sensitivity. The most parsimonious interpretation is that in a selenium-rich, but oxidatively challenged liver the capacity of GPX4 was the limiting factor rather than the signalling mediated by selenoprotein P, so the repletion of GPX4 capacity more than compensated for any cost of raising the level of selenoprotein P. That balance would not necessarily obtain at higher doses or in selenium-replete, metabolically healthy animals. The clinical relationship is itself less consistent than the mechanistic account implies: in a separate cohort of patients with type 2 diabetes, serum selenoprotein P showed no association with fasting insulin or with QUICKI, correlating instead inversely with adiponectin [35]. That serum concentrations track insulin resistance imperfectly weakens the inference that a rise in circulating selenoprotein P must carry a metabolic cost, and is consistent with the present observation that it rose alongside improved rather than worsened insulin sensitivity.

FGF21/β-Klotho and irisin/FNDC5 axes

Serum FGF21 was elevated almost threefold in the model (587 [421-794] versus 203 [158-261] pg/mL) alongside a 3.1-fold increase in hepatic *Fgf21* transcript — the pattern anticipated of a resistant rather than a deficient state, and the signature from which the concept of FGF21 resistance in obesity arose [36, 37] (Table 3). SeNPs 0.5 mg/kg reduced serum FGF21 to 312 [231-418] pg/mL and hepatic transcript to 1.71 ± 0.62-fold while elevating hepatic β-Klotho protein from 0.52 ± 0.15 to 0.84 ± 0.18 of control. The direction of these two changes taken together, corroborated by an inverse correlation between serum FGF21 and hepatic β-Klotho across the cohort ($r = -0.58$, $P < 0.001$; $n = 54$, that is all seven groups at the end of week 14), is what distinguishes relief of resistance from simple suppression of ligand production.

Interpretation of FGF21 resistance has been contested, and with reason: although β-Klotho protein declines in white adipose tissue during diet-induced obesity, restoring its expression at that site rescues neither FGF21 signalling nor sensitivity, so downregulation of the co-receptor is not the sole mechanism [38, 39]. The present data speak to the hepatic rather than the adipose arm. Falling ligand accompanied by rising co-

CC BY

receptor is the direction anticipated when a resistant state eases, and the opposite of what simple suppression of FGF21 production would yield in isolation. The evidence nevertheless falls short of demonstrating restored FGF21 action: hepatic FGFR1c moved in the same direction but no contrast against the model survived correction (omnibus P = 0.021), and no FGF21 challenge test was performed, this being the design that current criteria for evaluating FGF21 sensitivity would require [40]. These results are therefore consistent with partial relief of FGF21 resistance without establishing it.

The muscle axis responded at the higher dose alone. Serum irisin recovered from 7.1 ± 2.4 to 10.4 ± 3.1 ng/mL in G4, muscle FNDC5 protein rising from 0.49 ± 0.16 to 0.85 ± 0.21 and *Ppargc1α* transcript from 0.51 ± 0.19 to 0.86 ± 0.27-fold, the three moving as a unit. Such a hierarchy is to be anticipated, since FNDC5 is a PGC-1α target and irisin its cleaved product [41], while irisin in turn improves glucose uptake and mitochondrial function in myotubes through p38-MAPK-PGC-1α signalling, reversing experimental insulin resistance [42]. A plausible reading holds that restored muscle GPX4 activity shielded the PGC-1α-FNDC5 arm from oxidative suppression, which would then feed back upon insulin sensitivity. Two cautions apply. Irisin variance remained high relative to the effect size and the 0.25 mg/kg dose did not separate from the model; and adipose *Ucp1* rose numerically with treatment although the omnibus test was not significant after correction (P = 0.083), so the classical browning consequence of irisin signalling was not reproduced here and no thermogenic claim is supported by these data. The irisin findings are best regarded as a correlate of improved muscle redox status rather than as an identified effector.

Pre-specified contrasts, correlations and mediation

The central hypothesis was borne out by the planned comparisons (Table 6). Divergence of the model from control was apparent on all three primary axes, with a very large effect size for HOMA-IR (d = 3.3). SeNPs at 0.5 mg/kg produced a reduction in HOMA-IR of 4.39 units (95% CI −6.08 to −2.70; d = 2.5) together with an increase in hepatic GPX4 activity of 11.1 nmol/min/mg. Superiority of the nanoparticulate form over equimolar selenite was established for HOMA-IR (−2.42; 95% CI −3.98 to −0.86; P = 0.004), GPX4 activity (+7.8; P

Table 6. Pre-specified contrasts, correlations and mediation analysis.
The planned comparisons confirmed the main hypothesis: SeNPs no differently affected HOMA-IR, but GPX4 activity increased with SeNPs compared to ferrostatin-1, while selenite showed the opposite effect; GPX4 activity mediated 51% of the effect of SeNPs on HOMA-IR.

(a) Pre-specified contrasts - mean difference, 95% CI, Cohen's d (Holm correction)

Contrast	Purpose	HOMA-IR	d	P	Hepatic GPX4 activity	P	Hepatic MDA	P
G2 vs G1	Model validity	+5.58 (3.94 to 7.22)	3.3	< 0.001	−14.5 (−19.2 to −9.8)	< 0.001	+2.95 (2.01 to 3.89)	< 0.001
G4 vs G2	Principal effect	−4.39 (−6.08 to −2.70)	2.5	< 0.001	+11.1 (6.6 to 15.6)	< 0.001	−2.39 (−3.37 to −1.41)	< 0.001
G4 vs G5	Nano vs selenite	−2.42 (−3.98 to −0.86)	1.6	0.004	+7.8 (3.1 to 12.5)	0.002	−1.47 (−2.41 to −0.53)	0.006
G4 vs G6	Mechanistic equivalence	−0.31 (−1.38 to +0.76)	0.3	0.56	+10.3 (5.9 to 14.7)	< 0.001	−0.14 (−0.87 to +0.59)	0.71
G7 vs G1	Safety	−0.17 (−0.72 to +0.38)	0.3	0.53	+4.4 (−1.3 to 10.1)	0.12	−0.13 (−0.60 to +0.34)	0.58

(b) Spearman correlations for the pooled high fat groups (G2-G6, n = 38)

Variable	With hepatic GPX4 activity, ρ (P)	With HOMA-IR, ρ (P)	With hepatic MDA, ρ (P)
HOMA-IR	−0.67 (< 0.001)	—	0.71 (< 0.001)
K_ITT	0.58 (< 0.001)	−0.74 (< 0.001)	−0.55 (< 0.001)
Hepatic labile Fe(II)	−0.61 (< 0.001)	0.59 (< 0.001)	0.66 (< 0.001)
Hepatic ACSL4	−0.54 (0.001)	0.52 (0.001)	0.63 (< 0.001)
Serum FGF21	−0.49 (0.002)	0.64 (< 0.001)	0.51 (0.001)
Hepatic β-Klotho	0.46 (0.004)	−0.57 (< 0.001)	−0.44 (0.006)
Serum irisin	0.41 (0.011)	−0.48 (0.002)	−0.37 (0.022)
Hepatic Se	0.72 (< 0.001)	−0.45 (0.005)	−0.53 (0.001)
Adiponectin	0.38 (0.019)	−0.56 (< 0.001)	−0.42 (0.009)

(c) Mediation: GPX4 activity → MDA → HOMA-IR (PROCESS model 4, 5000 bootstrap resamples)

Path	Standardized β	95% CI	P
a: GPX4 → MDA	−0.69	−0.83 to −0.52	< 0.001
b: MDA → HOMA-IR | GPX4	0.47	0.18 to 0.74	0.002
c: Total effect	−0.66	−0.82 to −0.47	< 0.001
c′: Direct effect | MDA	−0.34	−0.63 to −0.04	0.027
a × b: Indirect effect	−0.32	−0.54 to −0.13	—
Proportion mediated	49%	22% to 79%	—

Partial mediation; there is substantial direct effect, which means there are parallel pathways (NRF2, iron, inflammation). The conclusion was the same for a sensitivity analysis which included final body weight as a covariate (a × b = −0.28; 95% CI from −0.50 to −0.10).

CC BY

= 0.002), and malondialdehyde (−1.47; P = 0.006). Set against ferrostatin-1, SeNPs proved equivalent with respect to HOMA-IR (−0.31; 95% CI −1.38 to +0.76; P = 0.56) and malondialdehyde (P = 0.71), yet superior with respect to GPX4 activity (+10.3; P < 0.001). On all three measures the safety contrast returned a null result.

Across the pooled high-fat groups, an inverse correlation obtained between hepatic GPX4 activity and HOMA-IR (ρ = −0.67, P < 0.001) and a positive one with K_ITT (ρ = 0.58), whereas malondialdehyde correlated positively with HOMA-IR (ρ = 0.71). The strongest correlate of GPX4 activity proved to be hepatic selenium (ρ = 0.72, P < 0.001), establishing a direct link between the element delivered and enzyme function. Both labile iron and ACSL4 varied in step with peroxidation and insulin resistance alike, and the endocrine markers conformed to expectation, FGF21 correlating positively and β-Klotho, irisin, and adiponectin negatively with HOMA-IR.

Mediation analysis situated malondialdehyde between GPX4 activity and insulin resistance (Fig. 4). The path running from GPX4 activity to malondialdehyde was markedly negative (β = −0.69), malondialdehyde retained predictive value for HOMA-IR following adjustment for GPX4 (β = 0.47, P = 0.002), and 49% of the total effect was attributable to the indirect path (95% CI 22–79%). The direct effect was still significant after the mediation of malondialdehyde (c′ = −0.34, P = 0.027), such that about half of the relationship was independent of lipid peroxidation as measured here. Possible parallel pathways include NRF2-dependent transcriptional responses, iron-dependent signalling that is absent of peroxidation, and inflammatory pathways, with recovery of antioxidant capacity (SOD and catalase) and total antioxidant capacity (TAC) consistent with a broader redox response. Malondialdehyde is also an imperfect single mediator, as it is a downstream product of multiple peroxidation reactions, and thus the 49% figure should be interpreted as the percentage due to the reaction that has been measured. The analysis is based on the temporal assumption that it is impossible to test, and the inclusion of final body weight as a covariate did not change the result of the analysis (indirect effect = −0.28; 95% CI = −0.50 to −0.10), addressing confounding by adiposity but not reverse causation.

Position in the ferroptosis and metabolic disease literature

The present results are concordant with, and extend, pharmacological investigations in fatty liver disease. Liproxstatin-1 diminished hepatic lipid deposition, 4-hydroxynonenal, malondialdehyde, and insulin resistance in a high-fat/high-fructose murine model, whereas iron chelation administered alone mitigated inflammation while failing to correct either lipid deposition or insulin resistance [43] — an asymmetry mirroring the dissociation observed here between selenite and SeNPs. Ferroptosis inhibition has consequently been advanced as a therapeutic strategy in metabolic fatty liver disease [44]. The contribution of the present study lies in supplying a nutritional and mechanistically upstream route to the same endpoint: in place of trapping lipid radicals with a

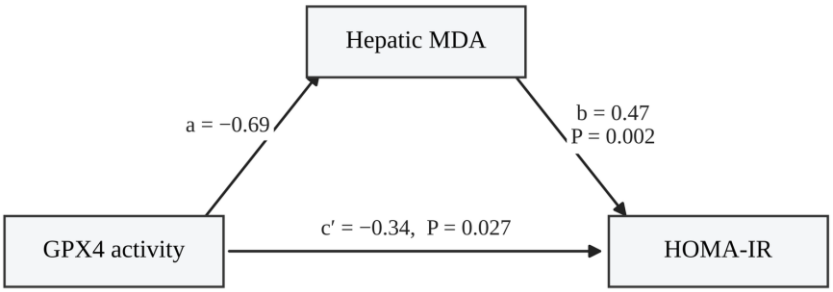


Fig. 4. Mediation of the relationship between hepatic GPX4 activity and insulin resistance by lipid peroxidation. Single-mediator model (PROCESS model 4, 5000 bootstrap resamples) fitted within the pooled high-fat groups (G2–G6, n = 38). Standardized path coefficients are shown. The indirect path accounted for 49% of the total effect (95% CI 22–79%) while the direct effect remained significant, indicating partial mediation.

CC BY

synthetic inhibitor, it reinstates the endogenous selenoenzyme whose failure licenses the chain reaction, and it establishes that the two approaches converge upon peroxidation and insulin sensitivity while diverging upon enzyme status.

The direction of the GPX4–insulin sensitivity relationship is nevertheless not uniform across tissues, and the present results should be read against that. Ferroptosis has recently been positioned as an integrating mechanism in the transition from insulin resistance to overt type 2 diabetes, linking lipotoxic substrate supply to regulated cell death [27]; the present work supplies an intervention aimed at the restraint arm of that axis. Yet deletion of *Gpx4* restricted to macrophages attenuated diet-induced obesity and improved insulin sensitivity in mice, with reduced systemic inflammation and adipocyte hypertrophy [26] — the opposite of what an undifferentiated reading of "more GPX4, better metabolism" would predict. The two findings are reconcilable only if the consequence of losing GPX4 depends on the cell in which it is lost: ferroptotic depletion of a pro-inflammatory macrophage population may relieve adipose inflammation, whereas loss of GPX4 in hepatocytes and myofibres, the compartments measured here, removes the restraint on peroxidation in the tissues that execute insulin action. Cell-specific heterogeneity of this kind is now explicit in the metabolic liver literature, where ferroptosis damages hepatocytes and sinusoidal endothelial cells and amplifies macrophage inflammation, yet is antifibrotic in activated stellate cells and immunosuppressive in lymphocytes [31]. Whole-tissue homogenates, as used here, cannot resolve that heterogeneity; they report the net balance across cell types. The present data therefore establish the direction of the net effect without identifying the cell in which it arises, and a cell-resolved study is the natural successor to this one.

Limitations

The conclusions are bounded by several constraints. Measurement ceased at week 14 with treatment still in progress, leaving untested the durability that ought to distinguish enzyme restoration from radical trapping. Characterization of the ferroptosis axis was biochemical in nature; neither mitochondrial ultrastructure, lipidomic profiling of oxidized phospholipid species, nor genetic manipulation of *Gpx4* was undertaken, with the consequence that ferroptotic cell death itself was not demonstrated directly. Given that effects separated between 0.25 and 0.5 mg Se/kg, the dose–response curve, the minimum effective dose, and the upper safety limit all remain undefined. Exposure, mediator, and outcome having been measured concurrently, the causal ordering within the mediation model is assumed rather than demonstrated. No exogenous FGF21 challenge was administered. Study of male rats of a single strain alone left unaddressed any sex differences in selenium metabolism, iron handling, and ferroptosis susceptibility, and findings obtained in a diet-induced rat model are not directly transferable to human insulin resistance. A single nanoparticle batch was administered to all animals, leaving batch-to-batch reproducibility untested; western blotting was conducted in five animals per group, and two groups concluded at n = 7.

The composition of the high-fat feed likewise qualifies comparison with the published literature. While the diet reproduced the 60:20:20 energy profile of the D12492 reference formulation, its fat was supplied as beef tallow and olive oil in place of lard and soybean oil, displacing the dietary fatty-acid profile toward monounsaturated and away from n-6 polyunsaturated species. Because ACSL4 esterifies polyunsaturated acyl chains into membrane phospholipids and thereby determines the substrate pool available for peroxidation [6, 7], dietary polyunsaturated fat supply is itself a determinant of ferroptosis susceptibility. Internal between-group comparisons remain unaffected, every high-fat group having received identical feed, but absolute peroxidation values are not directly comparable with studies employing the standard lard and soybean oil formulation. The locally prepared high-fat diet was formulated with reference to the D12492 dietary model; its final macronutrient composition and metabolizable energy content were not, however, independently verified by laboratory analysis. Potential discrepancies between intended and actual dietary composition therefore cannot be excluded, which may bear upon the standardization and reproducibility of the experimental insulin-resistance model; this limitation warrants consideration when the metabolic findings of the study are interpreted.

Three procedural limitations merit consideration as well. Humane endpoints had not been specified

CC BY

in advance by numerical thresholds, and the two animals lost during the treatment phase died spontaneously rather than being euthanized at a predetermined endpoint. Group variances were unequal for several outcomes, and although the analysis was repeated under procedures that do not assume homogeneity (section 3.9), the secondary outcomes most affected were those measured in the five-animal western-blot subset, where the loss of residual degrees of freedom leaves limited power. Laboratory assays, statistical analysis, and histological grading were all blinded to group identity and conducted on coded samples; direct physiological measurements in the live animal were, however, obtained in a fixed order by group rather than in randomized sequence, which admits a possible order effect in those in-vivo readings. Group size was not fixed by an a priori power calculation; the sensitivity analysis in section 3.9 shows the design to have been well powered for the primary and co-primary outcomes but not for small secondary effects. Lastly, although hepatic selenium was quantified, particle fate, the route of cellular uptake, and whether intact particles or released selenium species reached the target tissues were not established.

Sensitivity of the conclusions to the variance assumption and to study size

Group variances were not uniform across the seven arms. The ratio of the largest to the smallest group variance exceeded the conventional bound in three of the twenty-five normally distributed outcomes — fasting insulin, HOMA-IR and hepatic triglycerides — in each case because dispersion widened in the untreated model and selenite arms rather than because any single group was aberrant. The entire analysis was therefore repeated under procedures that assume neither equal variances nor equal group sizes.

The omnibus conclusions were unaffected for the primary and co-primary outcomes. Welch ANOVA returned $F(6, 19.9) = 15.2$ for HOMA-IR, $F(6, 20.8) = 14.8$ for hepatic GPX4 activity and $F(6, 20.3) = 11.3$ for hepatic malondialdehyde, all with $P < 0.001$, as did the equal-variance analysis. Three secondary outcomes did change status: the omnibus tests for HOMA-β ($P = 0.13$), transferrin receptor 1 ($P = 0.054$) and ferritin heavy chain 1 ($P = 0.16$) no longer reached significance. The latter two are western-blot outcomes measured in five animals per group, where the Welch correction to the residual degrees of freedom is most costly, and each is reported above as a directional pattern rather than as an established effect.

The five pre-specified contrasts, tested as Welch contrasts with Holm correction across the five, preserved every conclusion on which the argument of this paper rests. The model differed from control (HOMA-IR +5.58; 95% CI 3.44 to 7.72; $P = 0.003$). SeNPs at 0.5 mg Se/kg lowered HOMA-IR against the model (−4.39; 95% CI −6.56 to −2.22; $P = 0.007$) and against equimolar selenite (−2.42; 95% CI −4.21 to −0.63; $P = 0.042$), and raised hepatic GPX4 activity against both (+11.10; 95% CI 6.39 to 15.81; $P < 0.001$ and +7.80; 95% CI 2.84 to 12.76; $P = 0.010$). The contrast against ferrostatin-1 remained null for HOMA-IR (−0.31; 95% CI −1.42 to 0.80) and for malondialdehyde while remaining decisive for GPX4 activity (+10.30; 95% CI 5.59 to 15.01; $P = 0.001$), so the dissociation between repair of the enzyme and interception of lipid radicals is not an artefact of the variance assumption. The safety contrast was null on every measure.

From this reanalysis, one qualification results and is set out explicitly. Neither the improvement in HOMA-IR ($P = 0.12$) nor the hepatic GPX4 activity ($P = 0.055$) of the nanoparticulate form is significant when the same comparisons are made using an all-pairs Games-Howell procedure, which corrects for all twenty-one pairwise comparisons instead of the five comparisons specified a priori. The contrast was prespecified prior to any between-group comparisons explored, and is reported here under the confirmatory frame that is best suited for that kind of study; the between-group comparison of superiority of SeNPs over selenite is offered here as suggestive rather than confirmatory, and as noted above should be replicated in a study powered for this specific comparison.

There was no predetermined study size due to a power calculation and a sensitivity analysis was conducted to determine what the design could detect. At $\alpha = 0.05$ and 80% power with 7 groups and 54 animals involved, the lowest effect size that is detectable is Cohen $f = 0.54$ ($\eta^2 = 0.22$). The effect sizes observed were significantly larger for the primary and co-primary outcomes ($f = 1.37$ for HOMA-IR, 1.43 for hepatic GPX4 activity, and 1.25 for hepatic malondialdehyde), allowing for the study to be comfortably powered to detect the effects it was designed to detect. It was not

CC BY

designed for small secondary effects, and the three that became insignificant in the "welch" analysis fall into that category; none of them bear the argument.

CONCLUSION

Chitosan-stabilized selenium nanoparticles administered at 0.5 mg Se/kg reinstated hepatic GPX4 activity at 87% of control values, suppressed iron-dependent lipid peroxidation in liver and skeletal muscle alike, and reduced HOMA-IR by 58% in diet-induced insulin-resistant rats. The magnitude of effect surpassed that of an equimolar inorganic selenium salt on every primary axis while yielding a more favourable hepatic safety profile, establishing chemical form rather than selenium dose alone as the determinant of outcome. Relative to ferrostatin-1, SeNPs attained identical insulin-sensitivity and peroxidation endpoints through a distinct mechanism: restoration of the selenoenzyme in place of interception of lipid radicals downstream of it. These changes were accompanied at the higher dose by relief of hepatic FGF21 resistance and recovery of the muscle FNDC5/irisin axis. Since lipid peroxidation mediated only approximately half of the GPX4–insulin sensitivity relationship, parallel routes await identification. These findings establish engagement of the GPX4-dependent lipid-peroxidation axis; because the axis was characterized biochemically, they do not establish that ferroptotic cell death was occurring or that it was prevented. Direct lipidomic confirmation of oxidized phospholipid species, characterization of the dose–response relationship, a washout design to interrogate durability, and studies encompassing both sexes constitute the logical next steps.

ACKNOWLEDGEMENTS

The authors are grateful to the staff of the Laboratory Animal House and of the analytical laboratories of the State Company for Drugs Industry and Medical Appliances / Samarra (SDI) for their technical support.

CONFLICT OF INTEREST

The authors declare that there is no conflict of interests regarding the publication of this manuscript.

REFERENCES

1. Ibrahim SL, Al-Dawah NKJ, Al-Barqaawi MA. Comparative analysis of antioxidant status in diabetic patients with and without insulin resistance. J Med Life. 2023;16(9):1321-1326.
2. Hassan AB, Salih SF, Hassan II, Saadi FS, Abdulah DM, Ahmed IH, et al. Circulating betatrophin in relation to metabolic, inflammatory parameters, and oxidative stress in patients with type 2 diabetes mellitus. Diabetes and Metabolic Syndrome: Clinical Research and Reviews. 2019;13(1):458-463.
3. Ursini F, Maiorino M. Lipid peroxidation and ferroptosis: The role of GSH and GPx4. Free Radical Biology and Medicine. 2020;152:175-185.
4. Costa I, Barbosa DJ, Benfeito S, Silva V, Chavarria D, Borges F, et al. Molecular mechanisms of ferroptosis and their involvement in brain diseases. Pharmacology and Therapeutics. 2023;244:108373.
5. Xie Y, Kang R, Klionsky DJ, Tang D. GPX4 in cell death, autophagy, and disease. Autophagy. 2023;19(10):2621-2638.
6. Wu J, Minikes AM, Gao M, Bian H, Li Y, Stockwell BR, et al. Intercellular interaction dictates cancer cell ferroptosis via NF2–YAP signalling. Nature. 2019;572(7769):402-406.
7. Zeng K, Li W, Wang Y, Zhang Z, Zhang L, Zhang W, et al. Inhibition of CDK1 Overcomes Oxaliplatin Resistance by Regulating ACSL4-mediated Ferroptosis in Colorectal Cancer. Advanced Science. 2023;10(25).
8. Wenzel SE, Tyurina YY, Zhao J, St. Croix CM, Dar HH, Mao G, et al. PEBP1 Wardens Ferroptosis by Enabling Lipoxygenase Generation of Lipid Death Signals. Cell. 2017;171(3):628-641.e626.
9. Tong J, Lan X-t, Zhang Z, Liu Y, Sun D-y, Wang X-j, et al. Ferroptosis inhibitor liproxstatin-1 alleviates metabolic dysfunction-associated fatty liver disease in mice: potential involvement of PANoptosis. Acta Pharmacol Sin. 2022;44(5):1014-1028.
10. Ji J, Wu L, Wei J, Wu J, Guo C. The Gut Microbiome and Ferroptosis in MAFLD. Journal of Clinical and Translational Hepatology. 2022;000(000):000-000.
11. Misu H, Takamura T, Takayama H, Hayashi H, Matsuzawa-Nagata N, Kurita S, et al. A Liver-Derived Secretory Protein, Selenoprotein P, Causes Insulin Resistance. Cell Metab. 2010;12(5):483-495.
12. Takamura T. Hepatokine Selenoprotein P-Mediated Reductive Stress Causes Resistance to Intracellular Signal Transduction. Antioxidants and Redox Signaling. 2020;33(7):517-524.
13. Ojeda ML, Nogales F, Carreras O, Pajuelo E, Gallego-López MdC, Romero-Herrera I, et al. Different Effects of Low Selenite and Selenium-Nanoparticle Supplementation on Adipose Tissue Function and Insulin Secretion in Adolescent Male Rats. Nutrients. 2022;14(17):3571.
14. Abdulmalek SA, Balbaa M. Synergistic effect of nano-selenium and metformin on type 2 diabetic rat model: Diabetic complications alleviation through insulin sensitivity, oxidative mediators and inflammatory markers. PLoS One. 2019;14(8):e0220779.
15. Rabah HM, Mohamed DA, Mariah RA, Abd El-Khalik SR, Khattab HA, AbuoHashish NA, et al. Novel insights into the synergistic effects of selenium nanoparticles and metformin treatment of letrozole - induced polycystic ovarian syndrome: targeting PI3K/Akt signalling pathway, redox status and mitochondrial dysfunction in ovarian tissue.

Redox Report. 2023;28(1).
16. Zheng S, Hameed Sultan A, Kurtas PT, Kareem LA, Akbari A. Comparison of the effect of vitamin C and selenium nanoparticles on gentamicin-induced renal impairment in male rats: a biochemical, molecular and histological study. Toxicology Mechanisms and Methods. 2022;33(4):260-270.
17. Nafea MH, Jabir MS, Mohamemed AA, Al-kuraishy HM, Hasan AF, Ghotekar S, et al. Selenium nanoparticles-loaded with papain as a promising Nanoplatform for hepatocellular carcinoma control: 2D/3D tissue culture models and in silico prediction study. Int J Biol Macromol. 2025;330:147966.
18. Alkhalidi F. A comparative study to assess the use of chromium in type 2 diabetes mellitus. J Med Life. 2023;16(8):1178-1182.
19. Ahmad Tarmizi AA, Nik Ramli NN, Abdul Mutalib M, Jasmi NA, Mokhtar MH, Adam SH. Antioxidant and Hepatoprotective Effects of Moringa oleifera-mediated Selenium Nanoparticles in Diabetic Rats. F1000Research. 2025;14:7.
20. Flippo KH, Potthoff MJ. Metabolic Messengers: FGF21. Nature Metabolism. 2021;3(3):309-317.
21. Markan KR, Naber MC, Small SM, Peltekian L, Kessler RL, Potthoff MJ. FGF21 resistance is not mediated by downregulation of beta-klotho expression in white adipose tissue. Molecular Metabolism. 2017;6(6):602-610.
22. Markan KR. Defining "FGF21 Resistance" during obesity: Controversy, criteria and unresolved questions. F1000Research. 2018;7:289.
23. Chen N, Li Q, Liu J, Jia S. Irisin, an exercise-induced myokine as a metabolic regulator: an updated narrative review. Diabetes Metab Res Rev. 2015;32(1):51-59.
24. Ye X, Shen Y, Ni C, Ye J, Xin Y, Zhang W, et al. Irisin reverses insulin resistance in C2C12 cells via the p38-MAPK-PGC-1α pathway. Peptides. 2019;119:170120.
25. Piamsiri C, Maneechote C, Jinawong K, Arunsak B, Chunchai T, Chattipakorn SC, et al. Pharmacological inhibition of apoptosis, necroptosis, and ferroptosis confers effective cardioprotection in post-myocardial infarction in rats. Sci Rep. 2025;15(1).
26. Wu S, Peng J, Wang X, Gao H, Fang H, Hu S, et al. Gpx4 Deletion-Mediated Macrophage Ferroptosis Alleviates Obesity-Associated Insulin Resistance. The FASEB Journal. 2026;40(2).
27. Cui J, Li H, Liu J, Liu M, Zhao J. The lipotoxicity–ferroptosis axis in the transition from insulin resistance to type 2 diabetes: mechanistic integration and therapeutic opportunities. Front Endocrinol (Lausanne). 2026;17.
28. Wang Y, Zhang Z, Jiao W, Wang Y, Wang X, Zhao Y, et al. Ferroptosis and its role in skeletal muscle diseases. Frontiers in Molecular Biosciences. 2022;9.
29. Ding K, Liu C, Li L, Yang M, Jiang N, Luo S, et al. Acyl-CoA synthase ACSL4: an essential target in ferroptosis and fatty acid metabolism. Chin Med J. 2023;136(21):2521-2537.
30. Wu L, Lai W, Li L, Yang S, Li F, Yang C, et al. Autophagy Regulates Ferroptosis-Mediated Diabetic Liver Injury by Modulating the Degradation of ACSL4. Journal of Diabetes Research. 2024;2024(1).
31. Kotlyarov S, Iskrina A, Kotlyarova A. Ferroptosis in metabolic dysfunction-associated steatotic liver disease. Front Immunol. 2026;17.
32. Malyugina S, Skalickova S, Skladanka J, Slama P, Horky P. Biogenic Selenium Nanoparticles in Animal Nutrition: A Review. Agriculture. 2021;11(12):1244.
33. Misu H, Ishikura K, Kurita S, Takeshita Y, Ota T, Saito Y, et al. Inverse Correlation between Serum Levels of Selenoprotein P and Adiponectin in Patients with Type 2 Diabetes. PLoS One. 2012;7(4):e34952.
34. Dixon Scott J, Lemberg Kathryn M, Lamprecht Michael R, Skouta R, Zaitsev Eleina M, Gleason Caroline E, et al. Ferroptosis: An Iron-Dependent Form of Nonapoptotic Cell Death. Cell. 2012;149(5):1060-1072.
35. Yang Wan S, SriRamaratnam R, Welsch Matthew E, Shimada K, Skouta R, Viswanathan Vasanthi S, et al. Regulation of Ferroptotic Cancer Cell Death by GPX4. Cell. 2014;156(1-2):317-331.
36. Friedmann Angeli JP, Schneider M, Proneth B, Tyurina YY, Tyurin VA, Hammond VJ, et al. Inactivation of the ferroptosis regulator Gpx4 triggers acute renal failure in mice. Nat Cell Biol. 2014;16(12):1180-1191.
37. Doll S, Proneth B, Tyurina YY, Panzilius E, Kobayashi S, Ingold I, et al. ACSL4 dictates ferroptosis sensitivity by shaping cellular lipid composition. Nat Chem Biol. 2016;13(1):91-98.
38. Selmani A, Seibert E, Tetyczka C, Kuehnelt D, Vidakovic I, Kornmueller K, et al. Thiolated Chitosan Conjugated Liposomes for Oral Delivery of Selenium Nanoparticles. Pharmaceutics. 2022;14(4):803.
39. Wallenberg M, Olm E, Hebert C, Björnstedt M, Fernandes Aristi P. Selenium compounds are substrates for glutaredoxins: a novel pathway for selenium metabolism and a potential mechanism for selenium-mediated cytotoxicity. Biochemical Journal. 2010;429(1):85-93.
40. Welch BL. ON THE COMPARISON OF SEVERAL MEAN VALUES: AN ALTERNATIVE APPROACH. Biometrika. 1951;38(3-4):330-336.
41. Games PA, Howell JF. Pairwise Multiple Comparison Procedures with Unequal N's and/or Variances: A Monte Carlo Study. Journal of Educational Statistics. 1976;1(2):113-125.
42. Correction: An Improved Sequentially Rejective Bonferroni Test Procedure. Biometrics. 1987;43(3):737.
43. Benjamini Y, Hochberg Y. Controlling the False Discovery Rate: A Practical and Powerful Approach to Multiple Testing. Journal of the Royal Statistical Society Series B: Statistical Methodology. 1995;57(1):289-300.
44. Bolin JH. Hayes, Andrew F. (2013). Introduction to Mediation, Moderation, and Conditional Process Analysis: A Regression-Based Approach. New York, NY: The Guilford Press. Journal of Educational Measurement. 2014;51(3):335-337.

CC BY